Energy Conversion and Management 103 (2015) 374–386

Contents lists available at ScienceDirect

Energy Conversion and Management

journal homepage: www.elsevier.com/locate/enconman

Annual energy analysis of concrete containing phase change materials for building envelopes

Alexander M. Thiele [a], Astrid Jamet [a], Gaurav Sant [b,c], Laurent Pilon [a,*]

[a] Mechanical and Aerospace Engineering Department, Henry Samueli School of Engineering and Applied Science, University of California, Los Angeles, United States
[b] Civil and Environmental Engineering Department, Laboratory for the Chemistry of Construction Materials (LC^2), University of California, Los Angeles, United States
[c] California Nanosystems Institute (CNSI), University of California, Los Angeles, United States

ARTICLE INFO

Article history:
Received 23 December 2014
Accepted 22 June 2015

Keywords:
Phase change materials
Microencapsulated
Composite walls
Energy efficient building
Annual
Cost-savings

ABSTRACT

This paper examines the annual energy and cost savings potential of adding microencapsulated phase change material to the exterior concrete walls of an average-sized single family home in California climate zones 3 (San Francisco, CA) and 9 (Los Angeles, CA). The annual energy and cost savings were larger for South- and West-facing walls than for other walls. They were also the largest when the phase change temperature was near the desired indoor temperature. The addition of microencapsulated phase change material to the building walls reduced the cooling load in summer substantially more than the heating load in winter. This was attributed to the cold winter temperatures resulting in nearly unidirectional heat flux on many days. The annual cooling load reduction in an average-sized single family home in San Francisco and in Los Angeles ranged from 85% to 100% and from 53% to 82%, respectively, for phase change material volume fraction ranging from 0.1 to 0.3. The corresponding annual electricity cost savings ranged from $36 to $42 in San Francisco and from $94 to $143 in Los Angeles. From an energy standpoint, the best climate for using building materials containing uniformly distributed microencapsulated phase change material would have outdoor temperature oscillations centered around the desired indoor temperature for the entire year.

1. Introduction

In 2012, residential and commercial building operation represented about 29% of the total end-use energy consumed in California [1]. About 17% and 40% of this energy was consumed for space heating and air conditioning in commercial and residential buildings, respectively [2]. The demand of residential and commercial buildings for electricity varies significantly during the day [3]. To satisfy demand during peak hours, the utilities rely on so-called "*peaker plants*," which are costly to operate and typically run on fossil fuel [4]. In addition, utility companies offer time of use (TOU) electricity rate schedules to encourage ratepayers to shift their electricity use to off-peak hours. In practice, the price of electricity is lower during off-peak hours and higher during peak hours. Pacific Gas and Electric (PG&E) and the Los Angeles Department of Water and Power (LADWP) provide electricity with TOU rate schedules to San Francisco and Los Angeles, respectively. Together, they serve about 19 million residents or 50% of the California population. To curb the energy consumption of the building sector, the 2008 California long term energy efficiency strategic plan established two major objectives: (1) all new residential buildings should be zero net energy (ZNE) by 2020 and (2) all new commercial buildings by 2030 [5].

Minimizing the heat flow into and out of buildings is an important step toward achieving ZNE buildings [6]. Concrete containing microencapsulated phase change materials (PCMs) has been suggested as an envelope material to increase the buildings' thermal inertia and thus their energy efficiency [7,8]. PCMs store energy in the form of latent heat by reversibly changing phase between solid and liquid states. As a result, adding PCM to building walls reduces energy demand for heating and cooling and time-shifts the maximum daily thermal load on the building [9]. This can help ratepayers take advantage of TOU electricity rate schedules while reducing the ecological footprint of buildings [10]. The cost savings to the ratepayer depends both on the reduction and time-shift of the thermal load and on the TOU schedule [11].

The aim of the present study is to evaluate the potential annual energy and cost savings of adding microencapsulated PCM to the concrete-based building envelope of an average-sized single family home in California climate zones 3 (San Francisco, CA) and 9 (Los

* Corresponding author. Tel.: +1 (310) 206 5598; fax: +1 (310) 206 2302.
E-mail address: pilon@seas.ucla.edu (L. Pilon).

http://dx.doi.org/10.1016/j.enconman.2015.06.068
0196-8904/

Nomenclature

a	length of cubic unit cell, μm
AFUE	annual fuel utilization efficiency
A_j	area of wall with orientation "j", m^2
C_T, C_H, C_C	total, heating, and cooling cost, $
c_p	specific heat, J/kg K
D	unit-conversion constant, J Wh/BTU kW h
E_r	relative energy reduction, %
$H_H(q''_L), H_C(q''_L)$	heating and cooling heaviside step functions
h_i, h_o	indoor and outdoor convective heat transfer coefficient, W/m^2 K
h_{sf}	PCM latent heat of fusion, kJ/kg
k	thermal conductivity, W/m K
L	wall thickness, μm
Q	energy, J
Q''	energy flux, J/m^2
q''_s	solar radiation heat flux incident on the outer wall surface, W/m^2
q''_x, q''_y, q''_z	heat flux along the x-, y-, and z-directions, W/m^2
R_E	electricity rate, $/kW h
R_G	gas rate, $/J
S_T, S_H, S_C	total, heating, and cooling cost savings, $
SEER	seasonal energy efficiency ratio, BTU/Wh
t	time, s
T	temperature, °C
$T_{in}, T_\infty, T_{sky}$	indoor, ambient, and sky temperatures, °C
V_T	total volume of exterior walls, m^3

Greek symbols

α	thermal diffusivity, m^2/s
α_s	outer wall surface solar absorptivity
ΔT_{pc}	phase change temperature window, °C
ϵ	outer wall surface emissivity
ϕ	volume fraction
ρ	density, kg/m^3
σ	Stefan–Boltzmann constant, W/m^2 K^4

Subscripts

c	refers to core material (PCM)
eff	refers to effective properties
f	refers to final conditions
i	refers to initial conditions
j	refers to wall orientation "j" where $j = \mathrm{N, S, E, or\ W}$
l	refers to PCM liquid phase
L	refers to values at $x = L$
m	refers to matrix (concrete)
N, E, S, W	refers to North, South, East, and West wall orientations
o	refers to values at $x = 0$
s	refers to PCM solid phase or shell
pc	refers to phase change
T	refers to total quantities

Angeles, CA). The analysis was based on local annual weather data and on actual TOU electricity pricing.

2. Background

2.1. Experiments

The thermal response of concrete walls containing PCMs has been reviewed extensively [8,12–14]. In brief, most experimental studies of walls or rooms exposed to outdoor conditions have reported that adding PCM to building walls reduced the amplitude of the temperature oscillations at the wall surface and time-shifted the temperature peak. However, they did not quantify the corresponding energy savings [13].

Castellón et al. [7] constructed outdoor cubicles in Lleida, Spain made with (i) plain brick, (ii) plain brick with polyurethane insulation and 1.9 mass% macroencapsulated PCM with a melting temperature of 27 °C, (iii) alveolar brick, and (iv) alveolar brick containing 3.3 mass% macroencapsulated PCM with a melting temperature of 25 °C. The cubicles were equipped with a heat pump to maintain an indoor temperature of 24 °C. Their electricity consumption over the course of a summer week was reduced by up to 15% and 17% by adding PCM to the plain and alveolar brick cubicles, respectively. However, as acknowledged by the authors, the performance could be further improved by optimizing the PCM melting temperature. Such optimization would be costly and time consuming to perform experimentally. Moreover, it remains unclear whether these conclusions would be valid in other parts of the world with different climates. Rigorous numerical simulations can address these issues by assessing the effects of the climate conditions and of design parameters of PCM-composite walls such as the melting temperature and the PCM volume fraction on the thermal load of buildings in a rapid, systematic, and rational way.

2.2. Numerical simulations

Few studies have numerically investigated the transient thermal behavior of composite walls containing PCMs subjected to realistic boundary conditions based on weather data over an entire year [15–18]. In these studies, the inner wall surface was subjected to convective heat transfer to a constant indoor temperature [15–17] or to a temperature computed based on an energy balance of the indoor space [18]. The outer wall surface was subjected to both convective and radiative heat transfer with outdoor temperature and solar radiation heat flux from weather data over an entire year.

Kissock and Limas [15] solved the transient 1D heat diffusion equation in a 30.4 cm thick South-facing multilayer wall in Dayton, OH consisting of an insulation layer sandwiched between two concrete layers imbibed with 10 mass% paraffin PCM. The wall effective specific heat was determined by a weighted average of the concrete specific heat and the temperature-dependent PCM specific heat. The authors centered the phase change peak of the PCM specific heat curve at the desired indoor temperature. The maximum and annual cooling loads were reduced by 19% and 13%, respectively. On the other hand, the maximum and annual heating loads were reduced by only 11% and 1%, respectively. Note that directly imbibing concrete with PCM is neither realistic nor durable as the PCM reacts chemically with the cement which contains a pore-fluid with high pH ($pH > 13$) [19]. Thus, PCM should be encapsulated or contained [8,19].

Similarly, Mathieu-Potvin and Gosselin [16] simulated 1D heat transfer through a 10 cm thick South-facing wall in Quebec City, Canada comprised of polystyrene insulation with a single 0.5 cm thick pure PCM layer located near its center. They showed that the annual thermal energy flux through the PCM composite wall was minimized when the phase change temperature was near the desired indoor temperature. The PCM composite wall reduced the annual thermal load by about 7% compared with a slab of pure

polystyrene insulation of identical thickness. Here also, the PCM composite wall was found to reduce the cooling load in the summer substantially more than the heating load in the winter. Finally, the authors stated that there was no opportunity to optimize the energy reduction using a PCM layer if the wall heat flux was unidirectional, such as in Quebec City during the heating season (winter).

Zwanzig et al. [17] simulated a four-wall building in Minneapolis, MN, Louisville, KY, or Miami, FL consisting of 15.3 cm thick walls and a 12.4 cm thick flat ceiling of conventional multilayer construction. The walls and ceiling each contained a 1.3 cm thick layer of gypsum wallboard impregnated with 25 vol.% paraffin PCM featuring a phase change temperature window between 25 and 27.5 °C. The effective density and specific heat of the PCM wallboard layers were both determined by a weighted average using the mass fractions of PCM and gypsum. The effective thermal conductivity was determined using the Maxwell Garnett effective medium approximation (EMA) for inclusions in a continuous matrix. Adding PCM to the walls and ceiling reduced the thermal load on the building more during the cooling season (summer) than during the heating season (winter). The energy flux reduction through PCM composite walls depended on wall orientation due to differences in incident solar radiation heat flux.

Diaconu and Cruceru [18] simulated a building in Bechar, Algeria consisting of four multilayer walls each with a polystyrene insulation layer sandwiched between two PCM-wallboards. Each PCM-wallboard layer was assumed to be homogeneous with some arbitrarily chosen effective thermal properties. The authors found that the annual total cooling and heating loads were reduced by up to 1% and 13%, respectively, when the phase change temperature of PCM within the outer and inner layers was near the desired indoor temperature. However, the conclusions contradict those of other studies [15–17] who reported that the cooling energy savings was larger than the heating energy savings. We speculate that this discrepancy was due to the fact that climate conditions in Algeria resulted in a unidirectional wall heat flux during a large portion of the summer but not during the winter.

Few studies have evaluated the cost benefit of adding PCMs to residential building envelopes [20,21]. Chan [20] found that adding a shape stabilized PCM (SSPCM) layer to the West-facing wall of a residential flat in Hong Kong reduced the summer cooling load by 2.9%. Based on the material and installation cost, the author concluded that the payback period was excessively long, assuming a flat electricity rate. Here also, the small cooling load reduction may be due to unidirectional heat flux, since the outdoor temperature in Hong Kong often remains above 28 °C for the entire day in the summer [20].

Overall, the literature reported contradictory conclusions when comparing the energy saving potential of PCM composite walls during the winter and summer seasons. Moreover, the studies concerning PCM composite walls subjected to actual weather conditions either (i) neglected to account for the effects of PCM on the effective thermal conductivity and/or on the density of the composite walls [15], (ii) used EMAs that have not been validated [17], or (iii) the source or value of the effective thermal conductivity, effective density, and effective specific heat were not disclosed [18]. Most of the literature did not report the annual outdoor temperature used and/or the computed inner wall surface heat flux data which is important to understand the energy savings of PCM-composite walls. Finally, previous studies have not coupled the time shift of the heat transfer rate with a TOU electricity rate schedule to determine the associated cost savings.

2.3. Effective properties of three-component composites

Recently, we simulated time-dependent 3D heat transfer in three-component composite materials consisting of monodisperse or polydisperse microcapsules of PCM ordered or randomly distributed in a continuous matrix [9,22]. We showed that the temporal evolution of temperature and heat flux predicted within a homogeneous material with appropriate effective thermal properties agreed very well with that within a heterogeneous material with discrete core, shell, and matrix materials. The effective thermal conductivity k_{eff} was accurately predicted by the Felske model expressed as [23],

$$k_{eff}=\frac{2k_m(1-\phi_c-\phi_s)\left(3+2\frac{\phi_s}{\phi_c}+\frac{\phi_s k_c}{\phi_c k_s}\right)+(1+2\phi_c+2\phi_s)\left[\left(3+\frac{\phi_s}{\phi_c}\right)k_c+2\frac{\phi_s k_s}{\phi_c}\right]}{(2+\phi_c+\phi_s)\left(3+2\frac{\phi_s}{\phi_c}+\frac{\phi_s k_c}{\phi_c k_s}\right)+(1-\phi_c-\phi_s)\left[\left(3+\frac{\phi_s}{\phi_c}\right)\frac{k_c}{k_m}+2\frac{\phi_s k_s}{\phi_c k_m}\right]} \tag{1}$$

where k_c, k_s, and k_m are the thermal conductivities of the core, shell, and matrix, respectively, while ϕ_c and ϕ_s are the core and shell volume fractions. The effective volumetric heat capacity $(\rho c_p)_{eff}(T)$ was given by [9],

$$(\rho c_p)_{eff}(T)=\phi_c(\rho c_p)_c(T)+\phi_s(\rho c_p)_s+(1-\phi_c-\phi_s)(\rho c_p)_m \tag{2}$$

where $(\rho c_p)_c(T)$, $(\rho c_p)_s$, and $(\rho c_p)_m$ are the volumetric heat capacities of the core, shell, and matrix materials, respectively. According to the heat capacity method for simulating phase change, the volumetric heat capacity of the PCM $(\rho c_p)_c(T)$ was defined as a step function in terms of temperature with a rectangular peak of (i) width ΔT_{pc} centered around the phase change temperature denoted by T_{pc} and (ii) surface area equal to the PCM latent heat of fusion h_{sf} [9]. Thus, the effective volumetric heat capacity was also temperature-dependent and expressed as [9],

$$(\rho c_p)_{eff}(T)=\begin{cases}(\rho c_p)_{eff,s} & \text{for } T<T_{pc}-\Delta T_{pc}/2\\ (\rho c_p)_{eff,s}+\phi_c\frac{\rho_{c,s}h_{sf}}{\Delta T_{pc}} & \text{for } T_{pc}-\Delta T_{pc}/2\leqslant T\leqslant T_{pc}+\Delta T_{pc}/2\\ (\rho c_p)_{eff,l} & \text{for } T>T_{pc}+\Delta T_{pc}/2\end{cases} \tag{3}$$

where $(\rho c_p)_{eff,s}$ and $(\rho c_p)_{eff,l}$ are the effective volumetric heat capacity of the microencapsulated PCM-concrete wall when the PCM is solid and liquid, respectively. The heat capacity method (Eq. (3)) for simulating phase change was previously validated against the exact solution for the one-dimensional Stefan problem [9]. If the PCM is unmelted, then $(\rho c_p)_{eff,s}=\phi_c(\rho c_p)_{c,s}+\phi_s(\rho c_p)_s+(1-\phi_c-\phi_s)(\rho c_p)_m$ where $(\rho c_p)_{c,s}$ is the volumetric heat capacity of solid PCM. It was assumed to be equal to the effective volumetric heat capacity of the composite with fully melted PCM, i.e., $(\rho c_p)_{eff,s}=(\rho c_p)_{eff,l}$, as suggested from commercial organic PCM [24]. Note that this simplifying assumption has been widely used in the literature [18,25,26]. Here, T_{pc}, ΔT_{pc}, and h_{sf} represent the phase change temperature, temperature window, and latent heat of fusion, respectively. Note that the heat capacity method is an idealized representation of the PCM specific heat. In reality, PCMs exhibit superheating and subcooling during melting and freezing, respectively, delaying phase change and causing hysteresis in the $(\rho c_p)_c(T)$ vs. T plots. Eqs. (1)–(3) indicate that the effective thermal conductivity and effective volumetric heat capacity are independent of core and shell diameters, microcapsule spatial arrangement, and polydispersity, as established numerically [22].

The present study aims to use numerical simulations of a homogeneous wall with appropriate effective thermal properties subjected to realistic boundary conditions from weather data to evaluate the energy and cost saving associated with the use of microencapsulated PCM-concrete walls in a single family home in San Francisco and Los Angeles. First, the impact of wall orientation was elucidated. Second, the phase change temperature T_{pc} was varied to maximize energy and cost savings for a single family home in each climate. The heating, cooling, and total energy reductions and cost savings were compared both on a monthly and on an

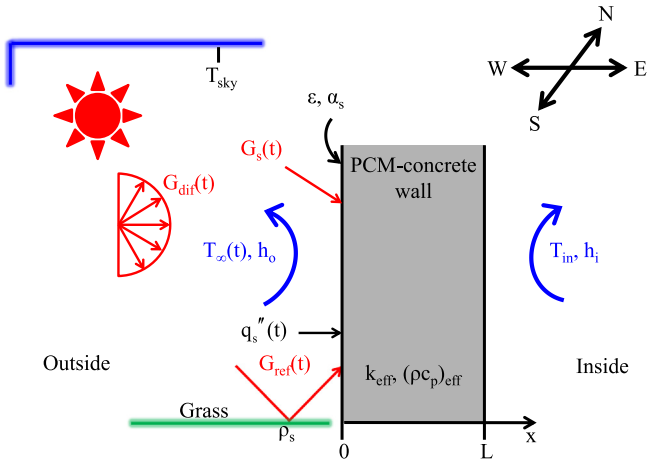

Fig. 1. Schematic of a homogeneous wall of thickness L with effective thermal conductivity k_{eff} and effective volumetric heat capacity $(\rho c_p)_{eff}$, representative of microencapsulated PCM-concrete. The wall was subjected to convection at the inside surface $(x = L)$ and to both convection and solar radiation heat flux at the outside surface $(x = 0)$.

annual basis. Finally, cost savings based on the noted TOU electricity rate schedules were discussed.

3. Analysis

3.1. Schematic and assumptions

Fig. 1 illustrates a microencapsulated PCM-concrete wall element of thickness $L = 10$ cm with effective thermal conductivity k_{eff} and effective volumetric heat capacity $(\rho c_p)_{eff}(T)$ given by Eqs. (1) and (3), respectively. The wall was subjected to convective heat transfer at the inside surface and to both convective and radiative heat transfer at the outside surface. The latter consisted of (i) diffuse and collimated solar radiation, (ii) radiation exchange with the sky, and (iii) solar radiation diffusely reflected by grass around the building. The variation of the solar radiation heat flux incident on the North, South, East, or West wall was also considered.

The home energy efficient design (HEED) software [27] compliant with the California Energy Commission procedures [28] was used to generate a reference simulation home that met California building code based on the average floor area of a single-family home of 240 m^2 (2600 ft^2) [29]. HEED determined the North and South wall areas to be 39.4 and 37.5 m^2, respectively, and both the East and West wall areas to be 27.9 m^2. These dimensions were used consistently in the present study. Note that the analysis did not account for the presence of windows or doors for the sake of simplicity.

To make the problem mathematically tractable, the following assumptions were made: (1) the microencapsulated PCM-concrete wall had isotropic and constant thermal properties except for the temperature-dependent effective specific heat (Eq. (3)), (2) the specific heat of the PCM was the same for the solid and liquid phases, i.e., $(\rho c_p)_{c,s} = (\rho c_p)_{c,l}$ so that $(\rho c_p)_{eff,s} = (\rho c_p)_{eff,l}$, (3) there was no heat generation in the wall, (4) the outer wall surfaces were treated as gray and diffuse, and (5) weekends and holidays had the same TOU electricity rate schedules as weekdays.

3.2. Governing equations

Under the above assumptions, the local wall temperature $T(x,t)$ at any time t and location x was governed by the one-dimensional (1D) transient heat conduction equation [30],

$$\frac{\partial T}{\partial t} = \alpha_{eff}(T)\frac{\partial T}{\partial x} \tag{4}$$

where $\alpha_{eff}(T) = k_{eff}/(\rho c_p)_{eff}(T)$ is the effective thermal diffusivity of the microencapsulated PCM-concrete wall. The effective thermal conductivity k_{eff} and effective volumetric heat capacity $(\rho c_p)_{eff}(T)$ were determined using Eqs. (1)–(3) described in Section 2.3 and validated using detailed numerical simulations as previously discussed [9,22].

3.3. Initial and boundary conditions

The initial temperature was assumed to be uniform throughout the material and equal to T_i, i.e.,

$$T(x,0) = T_i. \tag{5}$$

Convective heat transfer was imposed at the interior wall surface $(x = L)$ with a constant indoor temperature T_{in} maintained by the heating, ventilation, and air-conditioning (HVAC) system so that [16],

$$-k_{eff}\frac{\partial T}{\partial x}(L,t) = h_i[T(L,t) - T_{in}] \tag{6}$$

where h_i is the mixed convective heat transfer coefficient accounting for both forced and natural convections. Combined convective and radiative heat transfer was imposed at the exterior wall surface $(x = 0)$ such that [16,18],

$$-k_{eff}\frac{\partial T}{\partial x}(0,t) = h_o[T(0,t) - T_\infty(t)] + \alpha_s q_s''(t) - \epsilon\sigma\left[T(0,t)^4 - T_{sky}^4\right] \tag{7}$$

where h_o is the outdoor convective heat transfer coefficient, $T_\infty(t)$ and T_{sky} respectively represent the outdoor and average sky temperatures, $q_s''(t)$ is the solar radiation heat flux at time t, and σ is the Stefan–Boltzmann constant (i.e., $\sigma = 5.67 \times 10^{-8}$ W/m^2 K^4). In addition, α_s and ϵ are the total hemispherical solar absorptivity and emissivity of the outdoor wall surface, respectively. They typically differ since solar radiation is concentrated in the visible and near infrared while the outer wall surface emits radiation in the mid-infrared [30].

3.4. Constitutive relationships

The density, thermal conductivity, and specific heat of the PCM, shell, and matrix corresponded to those of a commercial organic PCM (PureTemp 20 by Entropy Solutions Inc., Plymouth, MN) [24], high density polyethylene (HDPE) [31], and concrete [30], respectively. Table 1 summarizes the thermophysical properties of these materials used to predict the effective thermal properties of the wall k_{eff} and $(\rho c_p)_{eff}$ according to Eqs. (1)–(3). In order to isolate the thermal effect of the PCM volume fraction ϕ_c, the shell volume fraction ϕ_s was kept constant and equal to 0.08. The volume fraction of core with respect to shell material, defined as $\phi_{c/s} = \phi_c/(\phi_c + \phi_s)$, ranged from about 55% to 79%, within a realistic range of microencapsulated PCMs [32]. In practice, this can be achieved by adjusting the inner and outer microcapsule diameters from about 9 to 13 μm and from about 11 to 14 μm, respectively.

Table 1
Density ρ, specific heat capacity c_p, and thermal conductivity k of PCM, high density polyethylene (HDPE), and concrete.

Material	Subscript	ρ (kg/m^3)	c_p (J/kg K)	k (W/m K)	Ref.
PCM	c	860	2590	0.21	[24]
HDPE	s	930	2250	0.49	[31]
Concrete	m	2300	880	1.4	[30]

The phase change temperature window ΔT_{pc} and the latent heat of fusion h_{sf} of the PCM were taken to be 3 °C and 180 kJ/kg, respectively. The resulting effective thermal conductivity k_{eff} decreased and the effective volumetric heat capacity $\rho c_p(T)_{eff}$ increased nearly linearly with PCM volume fraction ϕ_c increasing from 0.0 to 0.3. Thus, both the thermal resistance and the sensible heat storage capacity of the composite wall increased with the addition of PCM. Commercial microencapsulated PCMs are available with a wide variety of phase change temperatures but similar thermal properties. Indeed, the phase change temperature of paraffin PCMs can be adjusted by blending constituents with different alkane chain lengths [33]. In order to select the optimum material and elucidate the effects of phase change temperature T_{pc} on the annual energy and cost savings associated with PCM-concrete walls, it was treated as a parameter ranging from 10 to 25 °C.

The indoor heat transfer coefficient h_i was taken to be 8 W/m^2 K. This value was consistent with experimental measurements for mixed forced and natural convections on a vertical wall reported by Awbi and Hatton [34]. The outdoor heat transfer coefficient h_o was taken as 20 W/m^2 K, based on previous numerical simulations of walls exposed to outdoor weather conditions [26,35]. These values of indoor h_i and outdoor h_o heat transfer coefficients were very similar to those recommended by ISO standard 6946 of 7.7 and 25 W/m^2 K, respectively [36]. The total hemispherical solar absorptivity α_s and emissivity ϵ of the outer wall surface were taken as 0.26 and 0.9, respectively corresponding to the typical values of white paint [30]. Finally, the average sky temperature T_{sky} was taken as 2 °C throughout the year [30].

The outdoor temperature $T_\infty(t)$ and solar radiation heat flux $q''_s(t)$ used in Eq. (7) were obtained from Climate Consultant software [37] for North-, South-, East-, and West-facing vertical walls for a typical year in California climate zones 3 (San Francisco) and 9 (Los Angeles) in 1 h increments. Fig. 2a and b plot the outdoor temperature $T_\infty(t)$ as a function of time over the entire year in San Francisco and in Los Angeles, respectively. The average outdoor temperature is notably lower in San Francisco, particularly during the summer months. Similarly, Fig. 2c and d plot the total solar radiation heat flux $q''_s(t)$ incident on South-facing vertical wall as a function of time over the entire year in San Francisco and in Los Angeles, respectively.

3.5. Data processing

3.5.1. Energy savings

The relative energy reduction and the cost savings were used to evaluate the performance of microencapsulated PCM-concrete walls compared with that of plain concrete walls. First, the relative energy flux reduction $E''_{r,j}$ for a wall of orientation j was defined as the relative difference between the total thermal energy flux $Q''_{m,j}$ (in J/m^2) transferred through a plain concrete wall (both inward and outward) and that through a microencapsulated PCM-concrete wall Q''_j, for the same outdoor conditions and duration, expressed as,

$$E''_{r,j} = \frac{Q''_{m,j} - Q''_j}{Q''_{m,j}}. \tag{8}$$

Here, $Q''_{m,j}$ and Q''_j for a wall of orientation j were defined as,

$$Q''_{m,j} = \int_{t_i}^{t_f} \left|q''_{L,m,j}(t)\right| dt \quad \text{and} \quad Q''_j = \int_{t_i}^{t_f} \left|q''_{L,j}(t)\right| dt \tag{9}$$

where t_i and t_f are the initial and final times of interest (e.g., 1 month or 1 year).

The conductive heat fluxes (in W/m^2) at the inner surface located at $x = L$ for a plain concrete wall $q''_{L,m,j}$ and for a microencapsulated PCM-concrete wall $q''_{L,j}$ of orientation j were given by Fourier's law as,

$$q''_{L,m,j}(t) = -k_m \frac{\partial T_m}{\partial x}(L,t) \quad \text{and} \quad q''_{L,j}(t) = -k_{eff} \frac{\partial T}{\partial x}(L,t). \tag{10}$$

The absolute values of $q''_{L,m,j}(t)$ and $q''_{L,j}(t)$ in Eq. (9) were considered to account for the fact that there is an energy cost associated with maintaining the indoor temperature at T_{in}, regardless of the direction of the heat flux across the wall.

Similarly, the relative energy reduction E_r through all four vertical walls of the home was defined as the relative difference between the total thermal energy Q_m transferred through the walls made of plain concrete and through those made of microencapsulated PCM-concrete Q and was expressed as,

$$E_r = \frac{Q_m - Q}{Q_m}. \tag{11}$$

The total thermal energy Q_m through all four plain concrete walls and that through all four microencapsulated PCM-concrete walls Q of the home were given by,

$$Q_m = \sum_{j=N,S,E,W} Q''_{m,j} A_j \quad \text{and} \quad Q = \sum_{j=N,S,E,W} Q''_j A_j \tag{12}$$

where A_j is the surface area (in m^2) of the wall of orientation j.

Finally, the relative heating and cooling energy reductions, denoted by $E_{r,H}$ and $E_{r,C}$, for an entire home were expressed as,

$$E_{r,H} = \frac{Q_{H,m} - Q_H}{Q_{H,m}} \quad \text{and} \quad E_{r,C} = \frac{Q_{C,m} - Q_C}{Q_{C,m}}. \tag{13}$$

The total heating load $Q_{H,m}$ (in J) on a house with plain concrete walls or with microencapsulated PCM-concrete walls Q_H were defined as,

$$Q_{H,m} = \sum_{j=N,S,E,W} Q''_{H,m,j} A_j \quad \text{and} \quad Q_H = \sum_{j=N,S,E,W} Q''_{H,j} A_j \tag{14}$$

Here $Q''_{H,m,j}$ and $Q''_{H,j}$ are the heating energy fluxes through plain concrete and through microencapsulated PCM-concrete walls with orientation j and were expressed as,

$$Q''_{H,m,j} = \int_{t_i}^{t_f} H_H\left(q''_{L,m,j}\right)\left|q''_{L,m,j}(t)\right| dt \quad \text{and}$$
$$Q''_{H,j} = \int_{t_i}^{t_f} H_H\left(q''_{L,j}\right)\left|q''_{L,j}(t)\right| dt \tag{15}$$

where $H_H(q''_L)$ is a Heaviside step function for heating ($q''_L < 0$) given by,

$$H_H(q''_L) = \begin{cases} 1 & \text{if} \quad q''_L \leqslant 0 \\ 0 & \text{if} \quad q''_L > 0 \end{cases}. \tag{16}$$

Lastly, the total cooling load $Q_{C,m}$ and Q_C (in J) on a home with plain concrete and microencapsulated PCM-concrete walls were respectively defined as,

$$Q_{C,m} = \sum_{j=N,S,E,W} Q''_{C,m,j} A_j \quad \text{and} \quad Q_C = \sum_{j=N,S,E,W} Q''_{C,j} A_j. \tag{17}$$

Here, $Q''_{C,m,j}$ and $Q''_{C,j}$ are the associated cooling energy fluxes expressed as,

$$Q''_{C,m,j} = \int_{t_i}^{t_f} H_C\left(q''_{L,m,j}\right)\left|q''_{L,m,j}(t)\right| dt \quad \text{and}$$
$$Q''_{C,j} = \int_{t_i}^{t_f} H_C\left(q''_{L,j}\right)\left|q''_{L,j}(t)\right| dt \tag{18}$$

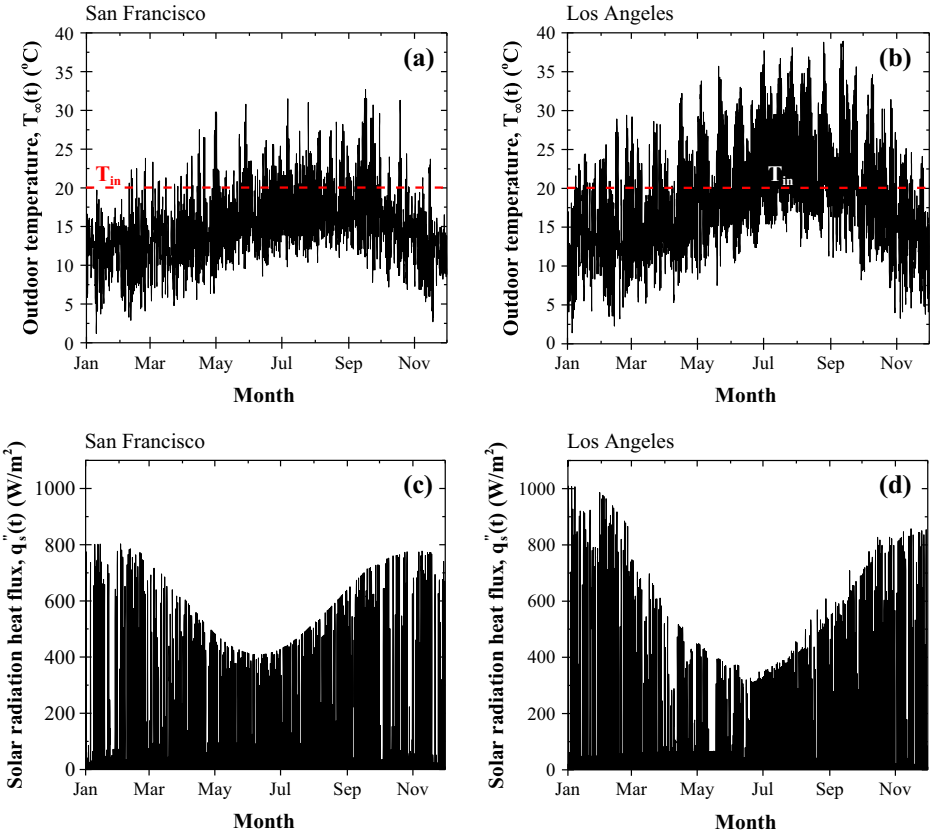

Fig. 2. (a) and (b) Outdoor temperature $T_\infty(t)$ and (c) and (d) solar radiation heat flux $q''_s(t)$ incident upon a South-facing vertical wall as functions of time throughout the year in San Francisco and in Los Angeles, respectively. These data were used as boundary conditions in the present study.

where $H_C(q''_L)$ is a Heaviside step function for cooling $(q''_L > 0)$ given by,

$$H_C(q''_L) = \begin{cases} 0 & \text{if} \quad q''_L \leqslant 0 \\ 1 & \text{if} \quad q''_L > 0 \end{cases}. \tag{19}$$

Note that the contributions to the thermal load from the roof or ceiling were assumed to be the same for the reference home with either concrete walls or microencapsulated PCM-concrete walls. Thus, they were not accounted for in the expressions of $E_r, E_{r,H}$, and $E_{r,C}$.

3.5.2. Cost savings

In order to determine the heating cost savings, the heating loads $Q_{H,m}$ and Q_H through the four walls were decomposed into off-peak and peak loads in the winter denoted by subscripts *op* and *p*. Similarly, the cooling loads $Q_{C,m}$ and Q_C were divided into off-peak, partial-peak, and peak loads denoted by subscripts *op*, *pp*, and *p*, in the summer, respectively. These TOU loads were isolated by adjusting t_i and t_f in Eq. (18) according to the summer or winter electricity rate schedules as defined by PG&E in San Francisco and by LADWP in Los Angeles.

An HVAC system was assumed to operate throughout the year with a tight constraint on the indoor temperature T_{in} such that it was constant and equal to 20 °C. Note, however that, in practice, the HVAC system would not activate until the room heated or cooled to a temperature outside a set comfort range, often called the temperature deadband. Thus, the heating and cooling energy requirements reported in the present study are overestimated. The seasonal energy efficiency ratio (SEER) is defined as the ratio of the total thermal energy removed from a space (in BTU) by an AC system to the electrical energy consumed over the same time period (in Wh) [38]. On the other hand, the annual fuel utilization efficiency (AFUE) is defined as the ratio of annual heat output by a furnace or boiler to the corresponding fossil fuel energy consumed [38]. In the present study, the current minimum value of SEER of 13 BTU/Wh set by the U.S. Department of Energy was used [38]. The average value of AFUE of 81 for modern furnaces and boilers was also used [38]. These values of SEER and AFUE were necessary in order to relate the cooling and heating loads to the corresponding electricity and gas consumption and to determine the associated costs.

The cost savings over a given time period, denoted by S_H, S_C, and S_T, were defined as the differences between the heating, cooling, and total costs (in \$) $C_{H,m}, C_{C,m}$, and $C_{T,m}$ when walls were made of plain concrete and C_H, C_C, and C_T when they were made of microencapsulated PCM-concrete. They were expressed as,

$$S_H = C_{H,m} - C_H, \quad S_C = C_{C,m} - C_C, \quad \text{and} \quad S_T = S_H + S_C. \tag{20}$$

Here, the heating and cooling costs C_H and C_C were given by,

$$C_H = \frac{1}{\text{AFUE}} Q_H R_G \quad \text{and}$$
$$C_C = \frac{1}{D \cdot SEER}\left[(Q_C R_E)_{op} + (Q_C R_E)_{pp} + (Q_C R_E)_p\right] \tag{21}$$

where $D = 1.055 \times 10^6$ J Wh/BTU kWh is a unit-conversion constant, R_G is the gas cost used for heating (in \$/J), and R_E is the electricity rate used for cooling (in \$/kW h). Eqs. (20) and (21) were applied both on a monthly and on an annual basis as well as both for individual walls and for all the walls in a home. Additionally, the cost savings through an individual wall with orientation *j* per unit wall area was given by $S''_{T,j} = S_{T_j}/A_j$.

3.6. Method of solution

The governing Eq. (4) along with the initial and boundary conditions given by Eqs. (5)–(7) were solved using finite element methods on unstructured grids. To account for the uncertainty in the initial conditions throughout the wall, the simulation time period was extended two days before January 1st. Extending the simulation period by an additional day resulted in less than 1% relative difference in temperature and heat flux predictions on January 1st. Numerical convergence was considered to be reached when the maximum relative difference in the predicted inner wall surface heat flux $q''_L(x,t)$ was less than 1% when reducing the mesh size or time step by a factor of 2. In practice, converged solutions were obtained by imposing a time step of 400 s and minimum mesh size and maximum growth rate to be 500 μm and 1.35, respectively. The number of finite elements needed to obtain a converged solution was 3233.

4. Results and discussion

4.1. Inner surface heat flux

Fig. 3 plots the inner surface heat flux $q''_{L,S}(t)$ as a function of time over one year for a South-facing wall located either in San Francisco (left) or in Los Angeles (right) with thermal properties corresponding to a plain concrete wall or to a concrete wall containing microencapsulated PCM with volume fraction ϕ_c ranging from 0.1 to 0.3. The phase change temperature T_{pc} was taken to be equal to the desired indoor temperature $T_{in} = 20\,^{\circ}\text{C}$. Fig. 3 shows that adding microencapsulated PCM to the concrete wall decreased the amplitude of the inner surface heat flux $q''_{L,S}(t)$ throughout the year. The amplitude of the positive heat flux $q''_{L,S}$ into the building requiring cooling was reduced substantially more than that of the heat flux out of the building (i.e., $q''_{L,S}(t) < 0$), requiring heating. Furthermore, the total thermal load was reduced much more during summer months when the temperature oscillations were centered closer to the desired indoor temperature T_{in}. This can be attributed to the fact that $q''_{L,S}$ was nearly unidirectional during the heating season (winter) in both cities but not during the cooling season (summer), as previously discussed. These results support recent findings that the energy reduction potential decreased as the difference between the time-averaged outdoor temperature and the desired indoor temperature T_{in} increased. Such situations are encountered in extremely hot or cold climates [9,16].

Fig. 4a–d plot the inner surface heat flux $q''_{L,m,S}(t)$ and the corresponding electricity rate $R_E(t)$ as functions of time over the course of one day for South-facing concrete walls located either in San Francisco or in Los Angeles on January 31st and on July 12th. The shaded areas below and above the line $q''_{L,m,S} = 0\ \text{W/m}^2$ respectively represent the daily heating $Q''_{H,m,S}$ and cooling energy fluxes $Q''_{C,m,S}$ required to maintain a constant indoor temperature T_{in}. The figures illustrate a general trend that buildings in Los Angeles require more cooling than those in San Francisco in both winter and summer due to the warmer climate (Fig. 2). They also show that the electricity providers in both cities divide the day into two and three pricing periods during the winter and summer, respectively. Summer pricing is applied from May to October in San Francisco and from June to September in Los Angeles. Moreover, the ratio of peak to off-peak electricity rates and the length of the peak period are larger in San Francisco than in Los Angeles. Fig. 4a presents the situation of unidirectional heat flux (heat loss) in San Francisco on January 31st.

4.2. Effect of wall orientation

Fig. 5a and b plot the annual relative energy flux reduction $E''_{r,j}$ achieved for the North-, South-, East-, and West-facing microencapsulated PCM-concrete walls as a function of PCM volume fraction ϕ_c ranging from 0 to 0.3 in San Francisco and in Los Angeles, respectively. Here also, the phase change temperature T_{pc} was taken to be equal to the desired indoor temperature T_{in} of 20 °C. First, it is evident that for every wall orientation, the annual energy flux reduction $E''_{r,j}$ increased with increasing PCM volume fraction ϕ_c. It was the largest for the West- and South-facing walls in San Francisco and Los Angeles, respectively, each reaching up to about 22% and 38%. This can be attributed to the fact that the solar radiation heat flux $q''_s(t)$ incident on the South- and West-facing walls resulted in oscillations in the inner wall surface temperature $T_L(t)$ centered closer to T_{in} than those at the East- and North-facing walls.

Fig. 5c and d plot the annual cost savings per unit surface area $S''_{T,j}$ of microencapsulated PCM-concrete wall (in $\$/\text{m}^2$ and in $\$/\text{ft}^2$) with different orientations corresponding to the energy savings presented in Fig. 5a and b. The annual cost savings per unit wall surface area $S''_{T,j}$ increased with increasing PCM volume fraction ϕ_c. It approached a plateau as ϕ_c increased above 15% in San Francisco for all four orientations considered. Here also, the West- and South- facings walls featured the largest cost savings $S''_{T,j}$ in both climates. However, the annual cost saving for the West-facing wall $S''_{T,W}$ was nearly equivalent to that for the South-facing wall $S''_{T,S}$ in Los Angeles, while it was larger by 30% in San Francisco.

Overall, Fig. 5a–d establish that the wall orientation had a substantial impact on the energy and cost savings associated with microencapsulated PCM-concrete walls in both San Francisco and Los Angeles. They also suggest that it may be more energy- and cost-effective to add microencapsulated PCM only to the West- and South-facing walls of a building envelope. Finally, adding PCM beyond ϕ_c of 0.1–0.2 in San Francisco would not make sense from a cost saving point of view although it was beneficial from an energy saving standpoint. Indeed, adding 10–20 vol.% microencapsulated PCM to the concrete walls time-shifted the maximum inner wall surface heat flux $q''_{L,j}(t)$ to a partial- or off-peak time of day with a cheaper electricity rate. Beyond this point, further increasing the time-shift by adding microencapsulated PCM resulted in proportionally less cost savings because the maximum energy consumption already occurred during the cheapest electricity rate period. This effect was much more pronounced in San Francisco since the ratio of peak to off-peak electricity rates was much larger than that in Los Angeles (Fig. 4).

4.3. Effect of phase change temperature

Fig. 6a and b respectively plot the relative energy reduction E_r and the associated cost savings S_T for the typical single family home considered for each month of the year in San Francisco achieved by adding 10 vol.% of PCM. Five different values of phase change temperature T_{pc} were considered, namely, 10, 19, 20, 21, and 25 °C. The results indicate that both E_r and S_T were maximized for $T_{pc} = 19\,^{\circ}\text{C}$. The monthly energy reduction ranged from about 6% to 17% throughout the year. The associated cost savings ranged from \$0.1/month in the winter to \$9/month in September. In fact, E_r and S_T were the smallest and were nearly independent of T_{pc} between November and March. This can be attributed to the fact that the inner wall surface heat flux was unidirectional $\left(q''_{L,j}(t) < 0\right)$ for most of this period, as previously discussed (Fig. 3). Throughout the year, E_r and S_T were almost equivalent

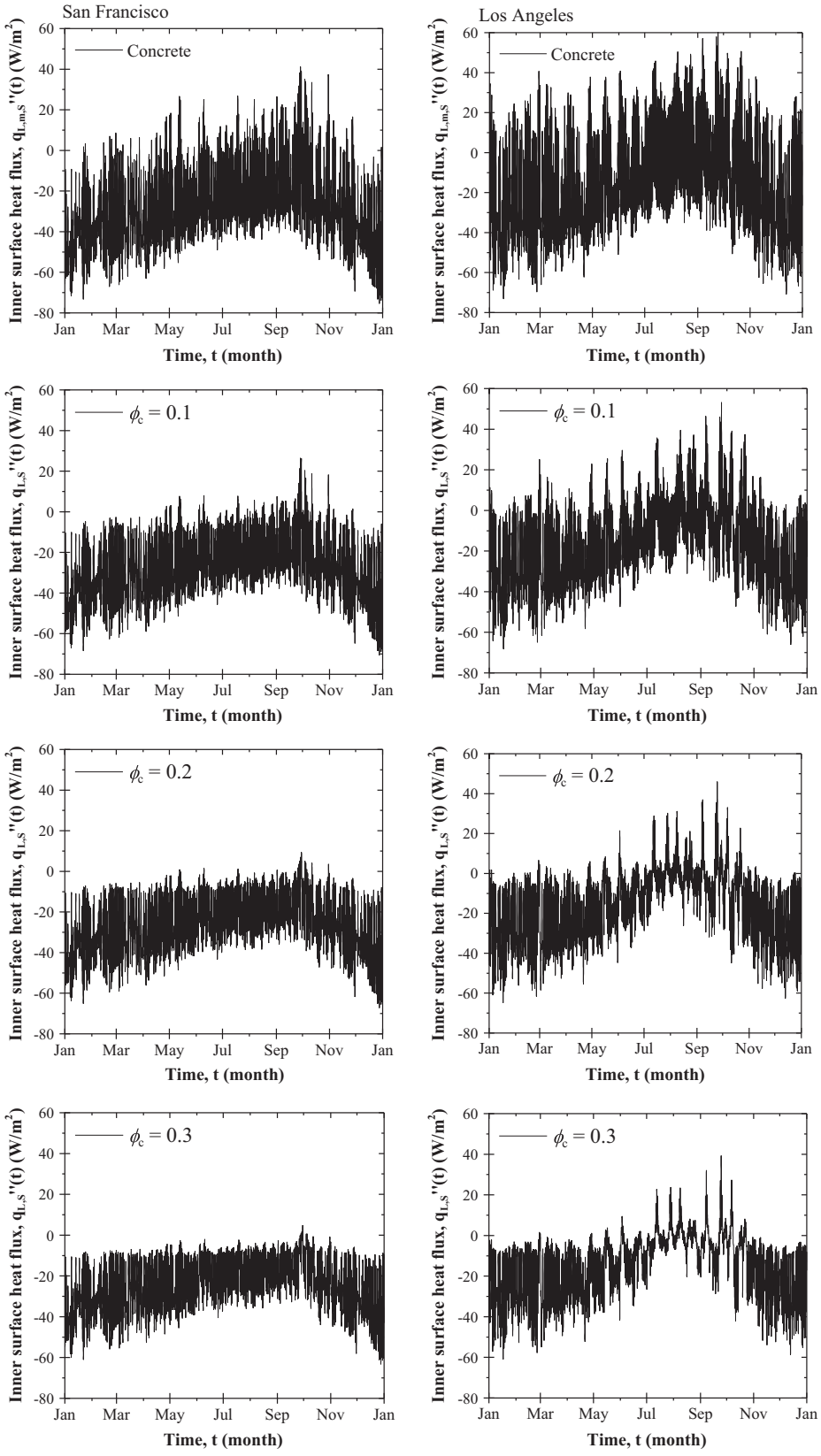

Fig. 3. Inner surface heat flux $q''_{LS}(t)$ as a function of time over one year for a South-facing plain concrete wall or for a microencapsulated PCM-concrete wall with PCM volume fraction ϕ_c ranging from 0.1 to 0.3 in San Francisco or in Los Angeles.

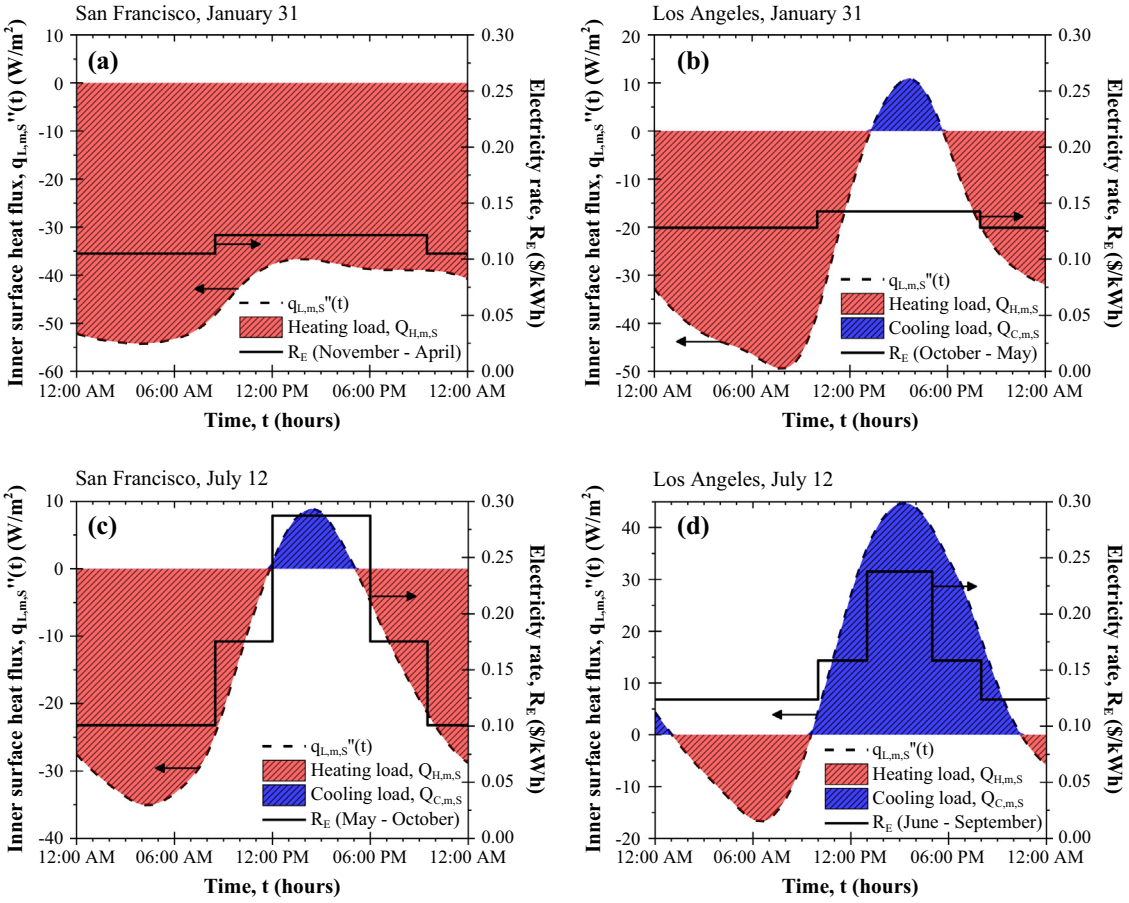

Fig. 4. Inner surface heat flux $q''_{L,m,S}(t)$ as a function of time for a South-facing plain concrete wall and the associated TOU electricity rate schedule on January 31 (winter) in (a) San Francisco and in (b) Los Angeles and on July 12 (summer) in (c) San Francisco and in (d) Los Angeles. The heating and cooling loads $Q_{H,m,S}$ and $Q_{C,m,S}$ are illustrated by the shaded area enclosed by the heat flux curve below and above $q''_{L,m,S} = 0$ W/m^2, respectively.

and equal to 6% for $T_{pc} = 10$ and 25 °C. This can be explained by the fact that the PCM remained liquid or solid on most days since the outdoor and the wall temperatures typically remained above 10 °C and below 25 °C (Fig. 2a), respectively. Then, the 6% energy reduction corresponding to T_{pc} of 10 and 25 °C can be attributed to the thermal insulating effects of adding the microencapsulated PCM, i.e., $k_{eff} < k_m$.

Similarly, Fig. 6c and d respectively plot E_r and S_T for the same typical home in Los Angeles, for each month of the year, for $\phi_c = 0.1$ and for T_{pc} ranging from 10 to 25 °C. They show that E_r and S_T reached a maximum in the summer months when the phase change temperature T_{pc} was equal to the desired indoor temperature T_{in} of 20 °C. However, both E_r and S_T were slightly larger for $T_{pc} = 19$ °C during the rest of the year. For $T_{pc} = 20$ °C, the relative energy reduction E_r ranged from 6% to 42% while the cost savings S_T varied from \$0.3 to \$21/month throughout the year. Here also, E_r and S_T were smaller and remained constant from October to May for $T_{pc} = 10$ and 25 °C. Then, the PCM did not completely change phase on most days and only the thermal insulating effects of the PCM microcapsules had an effect on the thermal load. Finally, the monthly cost savings was generally much larger in Los Angeles than in San Francisco. Note that the cost saving potential was limited by the cost of gas and electricity for heating and cooling the home under consideration.

4.4. Effect of season

Fig. 6a and c show that E_r was the largest during the summer months from June through September in both San Francisco and Los Angeles. This was due to the fact that the monthly time-averaged outdoor temperature $\overline{T}_\infty(t)$ in the summer months was 17 °C in San Francisco and 22 °C in Los Angeles. It was the closest to the desired indoor temperature $T_{in} = 20$ °C during these months.

Fig. 6b and d indicate that the cost savings S_T also reached a maximum during the summer months and was small in the winter months. In fact, the monthly cost savings in San Francisco was negligible between November and April. This was due to the fact that cooling was achieved by consuming electricity whose cost was based on summer TOU schedules featuring a large ratio of peak to off-peak electricity rates. By contrast, during the winter months, the heating load reduction was small and gas, sold based on a flat rate, was inexpensive.

Fig. 7a and b respectively compare E_r and S_T between San Francisco and Los Angeles for each month of the year for a PCM volume fraction $\phi_c = 0.2$. Here, T_{pc} was taken as 19 and 20 °C in San Francisco and in Los Angeles, respectively. The relative energy reduction E_r reached up to 23% and 62% and S_T reached up to \$11 and \$29/month in San Francisco and in Los Angeles, respectively. In addition, the monthly cost savings remained very small during the winter months in both cities. To put these numbers in perspective, the average monthly electricity bill over all residential customers in San Francisco and in Los Angeles between 1990 and 2005 was about \$70 and \$50/month, respectively [39]. Thus, adding 20 vol.% of microencapsulated PCM to the concrete walls of a single family home in Los Angeles resulted in up to ~60% cost savings in the summer months.

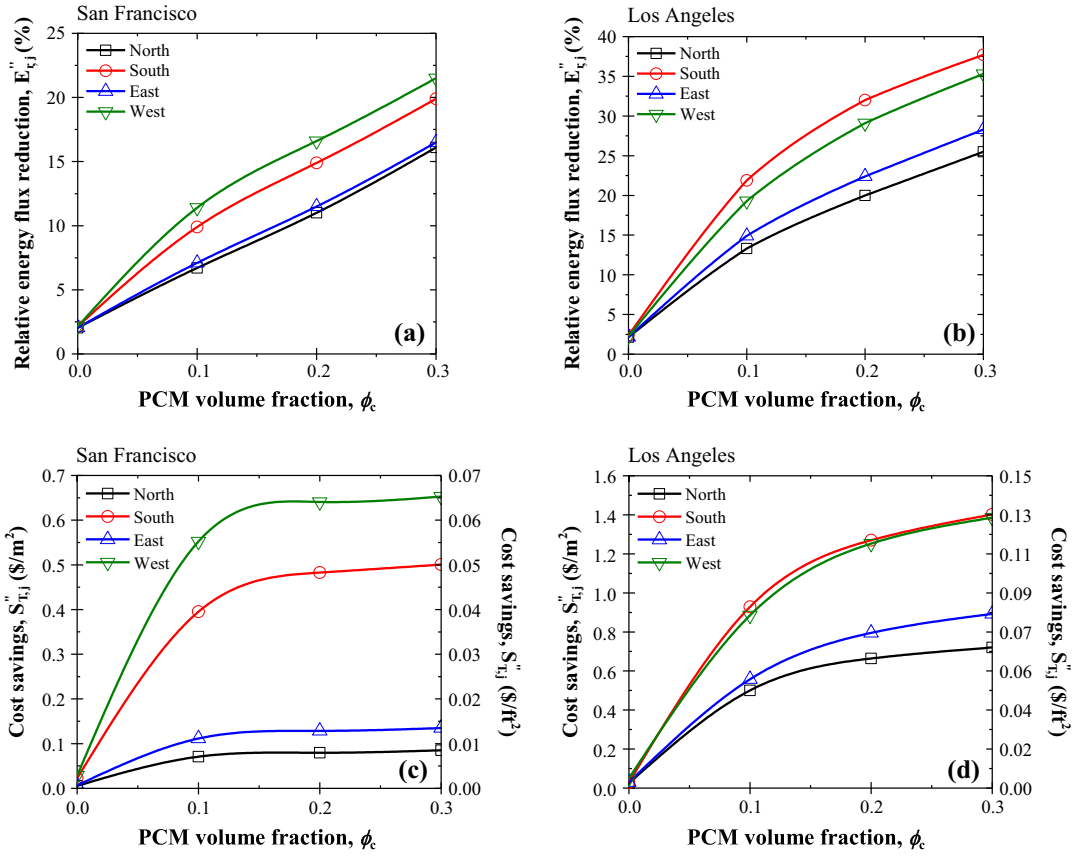

Fig. 5. Relative energy flux reduction $E''_{r,j}$ for North-, South-, East-, and West-facing walls (a) in San Francisco and (b) in Los Angeles, and corresponding cost savings per unit wall surface area $S''_{T,j}$ (c) in San Francisco and (d) in Los Angeles, as functions of PCM volume fraction ϕ_c ranging from 0 to 0.3.

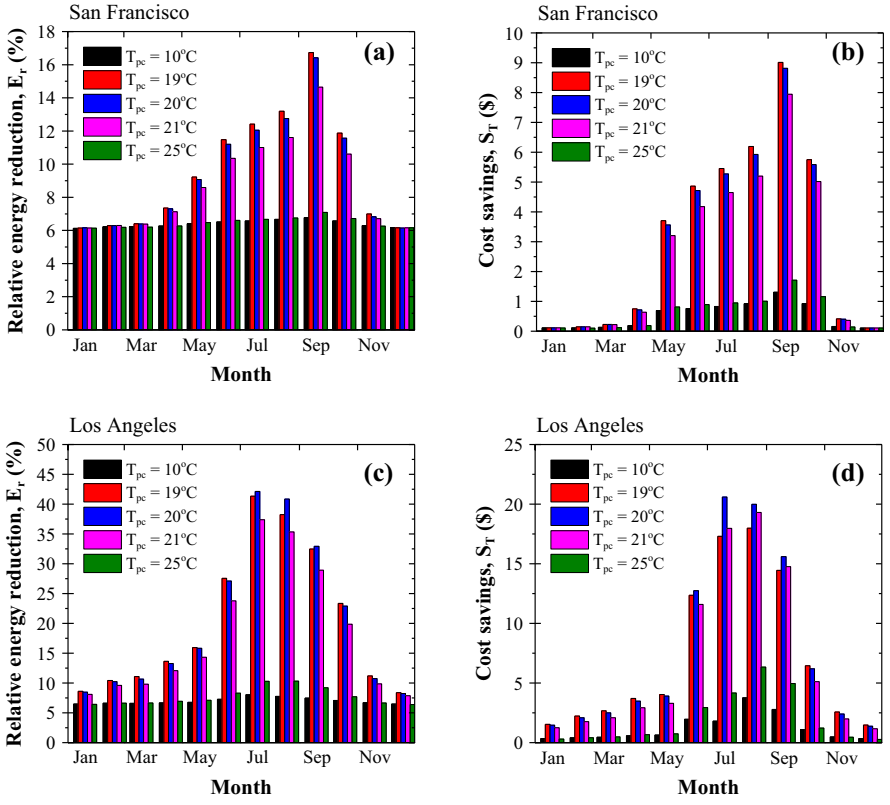

Fig. 6. (a) Relative energy reduction E_r and (b) cost savings S_T in San Francisco and (c) E_r and (d) S_T in Los Angeles for each month of the year for an average single family home. Here, $\phi_c = 0.1, h_{sf} = 180$ kJ/kg, $\Delta T_{pc} = 3$ °C, and the phase change temperature T_{pc} ranged from 10 to 25 °C.

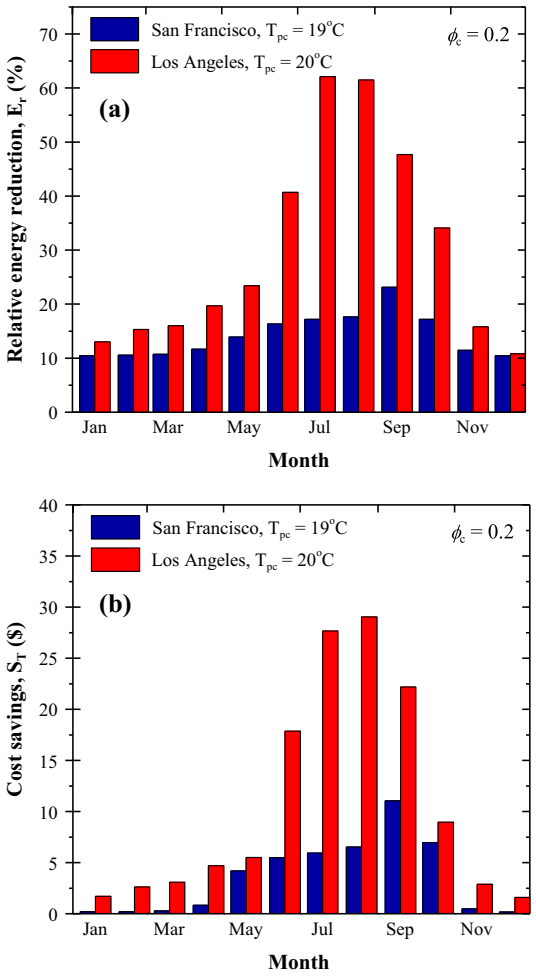

Fig. 7. Comparison of (a) the relative energy reduction E_r and (b) the cost savings S_T between San Francisco and Los Angeles for each month of the year for an average single family home. Here, $\phi_c = 0.2$, $h_{sf} = 180$ kJ/kg, $\Delta T_{pc} = 3$ °C, and T_{pc} was taken as 19 °C in San Francisco and 20 °C in Los Angeles.

4.5. Annual energy and cost savings

Table 2 shows the annual relative energy reduction for heating $E_{r,H}$, cooling $E_{r,C}$, and total E_r thermal loads on a typical single family home in San Francisco and Los Angeles. PCM volume fraction ϕ_c equal to 0.1, 0.2, and 0.3 was included either within all four walls of the home or strictly within the South- and West-facing walls as designated by "(PCM: S,W)." The annual cooling load was reduced by more than 98% in San Francisco and 73% in Los Angeles for ϕ_c above 0.2. However, the reduction in the annual heating load was comparatively small. The total annual relative energy reduction ranged from 9% to 18% in San Francisco and from 17% to 32% in Los Angeles as ϕ_c increased from 0.1 to 0.3. The comparative potential of a PCM-composite wall to reduce the heating or cooling loads individually depends on the climate. Overall, the best climate to reduce heat transfer by adding PCM to building walls is one in which the daily average outdoor temperature remains relatively close to the desired indoor temperature throughout the year, as in Los Angeles. Then, the heat flux through the inner surface of the walls changes direction during the day so that the PCM melts during the day and solidifies at night. Additionally, the total relative energy reduction E_r achieved by adding microencapsulated PCM only to the South- and West-facing walls of the home was significant but was only slightly more than half that achieved by including it within all four walls.

Table 2 also shows the annual cost savings S_T associated with the reduction in the heating, cooling, and total thermal loads in San Francisco and in Los Angeles for ϕ_c ranging from 0.1 to 0.3. In both cities, the annual cost savings consisted almost entirely of cooling cost savings in the form of electricity savings. Overall the total annual cost savings S_T ranged from \$37 to \$44 in San Francisco and from \$95 to \$145 in Los Angeles as ϕ_c increased from 0.1 to 0.3. Between 1990 and 2005, the average annual electricity cost for residential customers in San Francisco and Los Angeles was about \$840 and \$600, respectively [39]. Thus, the annual cost savings incurred by adding 20 vol.% microencapsulated PCM to concrete walls represented about 5% and 22% of the annual electricity expenditures in San Francisco and Los Angeles, respectively. Interestingly, the total annual cost savings S_T achieved by including

Table 2
Annual heating, cooling, and total relative energy reduction E_r and cost savings S_T for an average single family home in San Francisco and Los Angeles for different PCM volume fractions ϕ_c. Here, $h_{sf} = 180$ kJ/kg, $\Delta T_{pc} = 3$ °C, and $T_{pc} = 19$ °C in San Francisco and $T_{pc} = 20$ °C in Los Angeles.

	$\phi_c = 0.1$	$\phi_c = 0.2$	$\phi_c = 0.3$
Annual relative energy reduction (%)			
San Francisco			
$E_{r,H}$	7.5	12.0	17.0
$E_{r,C}$	85.1	98.3	99.6
E_r	8.8	13.4	18.3
E_r (PCM: S, W)	5.1	7.5	9.8
Los Angeles			
$E_{r,H}$	12.5	19.4	24.8
$E_{r,C}$	52.5	73.1	81.5
E_r	17.3	25.8	31.6
E_r (PCM: S, W)	10.3	15.2	18.1
Annual cost savings (\$)			
San Francisco (annual electricity cost: \$840)			
S_H	\$1	\$2	\$2
S_C	\$36	\$41	\$42
S_T	\$37	\$43	\$44
S_T (PCM: S, W)	\$31	\$36	\$37
Los Angeles (annual electricity cost: \$600)			
S_H	\$1	\$1	\$1
S_C	\$94	\$130	\$143
S_T	\$95	\$131	\$145
S_T (PCM: S,W)	\$60	\$83	\$91

microencapsulated PCM only within the South- and West-facing walls was only slightly smaller than that for four walls in San Francisco. This can be attributed to the very small annual cost savings for the North- and East-facing walls (Fig. 5c) in San Francisco. On the other hand, annual cost savings S_T were substantially smaller in Los Angeles when microencapsulated PCM was included only within the South- and West-facing walls. This suggests that the financial benefit of PCM-composite walls may be maximized in certain climates by careful and creative design choices such as the location of the PCM within the building envelope. In order to explore cost savings further, the material and implementation costs of PCM should be considered along with any incentive policies in order to assess the payback period for different PCM-composite building envelope designs.

5. Conclusion

This study demonstrated that adding miroencapsulated PCM to the exterior concrete walls of an average-sized single family residence can lead to significant annual energy savings both in San Francisco and in Los Angeles. Overall, the annual cooling load reduction ranged from 85% to 100% and from 53% to 82% in San Francisco and in Los Angeles, respectively, as the PCM volume fraction increased from 0.1 to 0.3. The corresponding annual electricity cost savings ranged from $36 to $42 in San Francisco and from $94 to $143 in Los Angeles. The present study also establishes that the location of PCM within the building envelope is an important design choice, particularly from a financial standpoint. Several important design guidelines for the PCM-composite wall system were obtained:

1. The annual energy reduction and cost savings were dependent on wall orientation, and were the largest for the South- and West-facing walls in the climates considered.
2. The annual energy and cost savings were maximized when the phase change temperature was near the desired indoor temperature.
3. Microencapsulated PCM reduces heat transfer through concrete walls the most in climates where the outdoor temperature oscillates around the desired indoor temperature.
4. Adding microencapsulated PCM to the building envelop can significantly reduce the need for cooling in the hotter months in the climates considered.
5. The effects of microencapsulated PCM on the energy needs for heating and the associated cost savings were small.

Future studies could assess creative design strategies for incorporating PCM into the building envelope and structure.

Acknowledgement

This manuscript was prepared as a result of work sponsored by the California Energy Commission (Contract: PIR:-12-032), the National Science Foundation (CMMI: 1130028) and the University of California, Los Angeles (UCLA). It does not necessarily represent the views of the Energy Commission, its employees, the State of California, or the National Science Foundation. The Energy Commission, the State of California, its employees, contractors, and subcontractors make no warranty, express or implied, and assume no legal liability for the information in this document; nor does any party represent that the use of this information will not infringe upon privately owned rights. This manuscript has not been approved or disapproved by the California Energy Commission nor has the California Energy Commission passed upon the accuracy or adequacy of the information in this report.

References

[1] U.S. Energy Information Administration. State energy data system; June 2014. <http://www.eia.gov/state/seds>.
[2] Itron Inc., California Commercial End Use Survey. Tech. rep. CEC-400-2006-005, California Energy Commission, Sacramento, CA; March 2006.
[3] Farid MM, Khudhair AM, Razack SAK, Al-Hallaj S. A review on phase change energy storage: materials and applications. Energy Convers Manage 2004;45(9):1597–615.
[4] Wells J, Haas D, et al. Electricity markets: consumers could benefit from demand programs, but challenges remain. Tech. rep. GAO-04-844, Government Accountability Office, Washington, DC; August 2004.
[5] California Public Utilities Commission. California Long Term Energy Efficiency Strategic Plan: achieving maximum energy savings in California for 2009 and beyond, California Public Utilities Commission, San Francisco, CA; September 2008.
[6] Heschong Mahone Group, Inc., et al. The road to ZNE. Tech. rep. PGE0327.01, Pacific Gas & Electric Company, Rancho Cucamonga, CA; December 2012.
[7] Castellón C, Castell A, Medrano M, Martorell I, Cabeza LF. Experimental study of PCM inclusion in different building envelopes. J Solar Energy Eng 2009;131(4):041006.
[8] Ling T-C, Poon C-S. Use of phase change materials for thermal energy storage in concrete: an overview. Constr Build Mater 2013;46:55–62.
[9] Thiele AM, Sant G, Pilon L. Diurnal thermal analysis of microencapsulated PCM-concrete composite walls. Energy Convers Manage; 2015.
[10] Zhu N, Ma Z, Wang S. Dynamic characteristics and energy performance of buildings using phase change materials: a review. Energy Convers Manage 2009;50(12):3169–81.
[11] Morgan S, Krarti M. Impact of electricity rate structures on energy cost savings of pre-cooling controls for office buildings. Build Environ 2007;42(8):2810–8.
[12] Jayalath A, Mendis P, Gammampila G, Aye L, Ngo T. Applications of phase change materials in concrete for sustainable built environment: a review. In: Proceedings of the international conference on structural engineering, construction, and management (ICSECM), Kandy, Sri Lanka, December 16–18; 2011. p. 1–13.
[13] Kuznik F, David D, Johannes K, Roux J-J. A review on phase change materials integrated in building walls. Renew Sustain Energy Rev 2011;15(1):379–91.
[14] Tyagi VV, Kaushik SC, Tyagi SK, Akiyama T. Development of phase change materials based microencapsulated technology for buildings: a review. Renew Sustain Energy Rev 2011;15(2):1373–91.
[15] Kissock K, Limas S. Diurnal load reduction through phase-change building components. ASHRAE Trans 2006:509–17.
[16] Mathieu-Potvin F, Gosselin L. Thermal shielding of multilayer walls with phase change materials under different transient boundary conditions. Int J Therm Sci 2009;48(9):1707–17.
[17] Zwanzig SD, Lian Y, Brehob EG. Numerical simulation of phase change material composite wallboard in a multi-layered building envelope. Energy Convers Manage 2013;69:27–40.
[18] Diaconu BM, Cruceru M. Novel concept of composite phase change material wall system for year-round thermal energy savings. Energy Build 2010;42(10):1759–72.
[19] Fernandes F, Manari S, Aguayo M, Santos K, Oey T, Wei Z, et al. On the feasibility of using phase change materials (PCMs) to mitigate thermal cracking in cementitious materials. Cem Concr Compos 2014;51:14–26.
[20] Chan ALS. Energy and environmental performance of building façades integrated with phase change material in subtropical Hong Kong. Energy Build 2011;43(10):2947–55.
[21] Kosny J, Shukla N, Fallahi A. Cost analysis of simple phase change material-enhanced building envelopes in southern US climates. Tech. rep. DOE/GO-102013-3692, Fraunhofer center for sustainable energy systems, prepared for the US DOE Building Technologies Program; 2013.
[22] Thiele AM, Kumar A, Sant G, Pilon L. Effective thermal conductivity of three-component composites containing spherical capsules. Int J Heat Mass Transfer 2014;73:177–85.
[23] Felske JD. Effective thermal conductivity of composite spheres in a continuous medium with contact resistance. Int J Heat Mass Transfer 2004;47:3453–61.
[24] PureTemp 20 technical information. Tech. rep., Entropy Solutions Inc., Minneapolis, MN; 2011.
[25] Pasupathy A, Velraj R, Seeniraj RV. Phase change material-based building architecture for thermal management in residential and commercial establishments. Renew Sustain Energy Rev 2008;12(1):39–64.
[26] Hembade L, Neithalath N, Rajan SD. Understanding the energy implications of phase-change materials in concrete walls through finite-element analysis. J Energy Eng 2013;140(1):04013009.
[27] UCLA Energy Design Tools Group. Home energy efficient design; 2014. <http://www.energy-design-tools.aud.ucla.edu>.
[28] California Energy Commission, residential alternative calculation method. Tech. rep. CEC-400-2013-003-CMF, California Energy Commission, Sacramento, CA; 2013.
[29] ‘‘American housing survey for the united states: 2011. Tech. rep. H150/11, U.S. Census Bureau, Washington, DC; 2013.
[30] Incropera FP, Lavine AS, DeWitt DP. Fundamentals of heat and mass transfer. New York City, NY: John Wiley & Sons; 2011.

[31] Typical engineering properties of high density polyethylene. Tech. rep., INEOS Olefins & Polymers USA, League City, TX; 2009.
[32] Sarier N, Onder E. Organic phase change materials and their textile applications: an overview. Thermochim Acta 2012;540:7–60.
[33] Ukrainczyk N, Kurajica S, Šipušić J. Thermophysical comparison of five commercial paraffin waxes as latent heat storage materials. Chem Biochem Eng Quart 2010;24(2):129–37.
[34] Awbi HB, Hatton A. Mixed convection from heated room surfaces. Energy Build 2000;32(2):153–66.
[35] Alawadhi EM. Thermal analysis of a building brick containing phase change material. Energy Build 2008;40(3):351–7.
[36] International Organization for Standardization. ISO standard 6946: building components and building elements: thermal resistance and thermal transmittance – calculation method; 2007.
[37] UCLA Energy Design Tools Group. Climate consultant; 2014. <http://www.energy-design-tools.aud.ucla.edu>.
[38] U.S. Department of Energy. Energy and water conservation standards and their compliance dates, 10 CFR 430.32; 2014. <http://www.ecfr.gov/>.
[39] Gorin T, Pisor K. California's Residential Electricity Consumption, prices, and bills, 1980–2005. Tech. rep. CEC-200-2007-018, California Energy Commission, Sacramento, CA; September 2007.